J Appl Electrochem (2014) 44:179–187
DOI 10.1007/s10800-013-0625-3

RESEARCH ARTICLE

Stacked-cup-type MWCNTs as highly stable lithium-ion battery anodes

Juchuan Li · Aman Preet Kaur · Mark S. Meier · Yang-Tse Cheng

Received: 26 May 2013 / Accepted: 3 September 2013 / Published online: 24 September 2013
© Springer Science+Business Media Dordrecht 2013

Abstract Stacked-cup type multiwall carbon nanotubes (MWCNTs) were synthesized by floating catalyst chemical vapor deposition methods. The materials were characterized using scanning electron microscopy (SEM), transmission electron microscopy (TEM), X-ray diffraction (XRD), Raman spectroscopy, and X-ray photoelectron spectroscopy (XPS). Electrochemical measurements showed that the stacked-cup-type MWCNTs as lithium-ion battery anode materials delivered a stable capacity of $\sim$310 mAh g^{-1} at a rate of C/2 to 300 cycles. Furthermore, the materials were very stable and the coulombic efficiency exceeded 99.9 % over more than 300 cycles. Stable materials structure and the solid electrolyte interphase films were the main reasons for the durable cycling behavior, as confirmed by ex situ TEM and Raman spectroscopy, as well as electrochemical impedance spectroscopy (EIS). The results indicated that the stacked-cup-type MWCNTs produced in this work are candidate materials for lithium-ion battery anodes.

Keywords Lithium-ion battery · Anode (negative electrode) · Multiwall carbon nanotubes (MWCNTs) · Electrochemical impedance spectroscopy (EIS)

1 Introduction

Presently, rechargeable lithium-ion batteries (LIBs) are considered the most promising energy storage technologies for electronic devices, portable power tools, hybrid and pure electric vehicles (HEVs and PEVs), as well as for stationary energy storage [1]. However, existing commercial LIBs do not fully meet the ever-growing performance demands, especially for HEVs and PEVs. LIBs with higher capacities, higher energy densities, longer cycle lives, better safety, and lower costs are needed [1–3].

Since the early 1990s, natural and artificial graphite have been commercially used as the anodes (negative electrodes) of rechargeable LIBs because of their stable cycling performance, low electrochemical potential upon lithium insertion and extraction, and relatively low cost [4–6]. However, the low capacity of graphite (372 mAh g^{-1}) is one of the bottle-necks facing advanced LIB technologies today. Elements that form high lithium content alloys are currently being extensively explored, such as Si, Sn, and Ge. The large volume changes during lithiation and delithiation of these elements cause cracks to form in the electrodes and, consequently, short cycle lives of batteries [7–9]. Strategies to overcome mechanical failure are required for these high capacity negative electrode materials to have commercial applications.

Besides graphite, other types of carbon are considered potential anode materials for LIBs, especially carbon nanotubes (CNTs), disordered carbon, and graphene. CNTs are highly promising because of their unique properties

Juchuan Li and Aman Preet Kaur have contributed equally to this work.

J. Li (✉) · Y.-T. Cheng
Department of Chemical and Materials Engineering, University of Kentucky, Lexington, KY 40506, USA
e-mail: jlin@g.uky.edu

Y.-T. Cheng
e-mail: yang.t.cheng@uky.edu

A. P. Kaur · M. S. Meier (✉)
Department of Chemistry, University of Kentucky, Lexington, KY 40506, USA
e-mail: mark.meier@uky.edu

including high aspect ratio, channels for intercalation of lithium, excellent electrical and thermal conductivities, and good mechanical properties [10, 11]. The reversible capacity of different kinds of CNTs ranges from 300 to 1,000 mAh g^{-1} [12–17], and is strongly dependent on their morphology, porosity, and chemical composition. The capacity of CNTs results from intercalation of Li atoms between the graphite layers and in the interstitial sites of close-packed CNT bundles, as well as from the effective diffusion into stable sites located on the nanotube surface and/or inside individual nanotubes through end caps or sidewall openings [18, 19]. Chemical and mechanical modifications, including chemical etching in acid solution [20], dicing long tubes into short segments [21], growing short tubes [22], and using vertically aligned CNTs [23], have been found effective in improving the electrochemical performance of CNTs in terms of capacity or cycle life.

Lin et al. [24] stated that Li diffuses or intercalates mainly into the graphite layers of multiwall carbon nanotubes (MWCNTs); the corresponding irreversible capacity results from Li storage in the hollow cores or the pores formed by entangled nanotubes. From theoretical modeling, Zhao et al. [25] proposed a mechanism of curvature-induced lithium condensation inside the core of the nanotubes. Liu et al. [26] observed the lithiation of individual MWCNT by in situ TEM, and reported lithiation-induced embrittlement of MWCNTs, a phenomenon that was attributed to the combined effects of mechanical and chemical weakening of the C–C bonds by Li insertion as well as the tensile hoop stress. Functionalization, such as the doping of CNT anodes with hetero-atoms, influences the Li storage capacity in CNTs. Nitrogen-doped MWCNTs (N-MWCNTs) have been investigated as anodes and have shown reversible capacity from 135 to 494 mAh g^{-1} [27–32]. Earlier reports showed that a capacity of more than 450 mAh g^{-1} and good cycling stability for up to 30 cycles could be achieved [27, 28]. The authors also observed lithium nanocrystallites directly inside the nanocavities of N-MWCNTs using TEM [27, 28]. Recent reports attributed higher reversible capacity of N-MWCNTs to the incorporation of graphitic or pyridinic N-atoms that facilitate electrical conductivity as well as the many defect sites for Li storage [30–32]. Although high capacity of MWCNTs can be reached by functionalizing the nanotubes, their capacity retention and cycle life are limited.

Besides lithium storage, CNTs can also be used to replace carbon black as conductive additives in composite electrodes, or used for active–active composite electrodes [33–37]. Due to the high aspect ratio, an electrical percolation network can be established with lower weight loading of CNTs than with conventional carbon black [29, 38–44]. For example, it has been shown that stable reversible capacity and significant improvement in rate performance of cathode materials can be achieved when 1.5 wt% of SWCNTs were added as the conducting additives [34]. Cathode materials, including $LiCoO_2$, $LiFePO_4$, and $LiNi_{0.7}Co_{0.3}O_2$, showed about 10 % improvement in reversible capacity when MWCNTs were used as additives instead of carbon black [39–41, 43].

In this paper, we report the fabrication of stack-cup type MWCNTs (SC-MWCNTs) and their lithium storage behavior. Our results show that a reversible capacity of $\sim$310 mAh g^{-1} and excellent coulombic efficiency of more than 99.9 % under a rate of C/2 can be achieved up to 300 cycles. The stability of SC-MWCNTs was examined using ex-situ TEM, Raman spectroscopy, and electrochemical impedance spectroscopy (EIS). The SC-MWCNTs in this study are potential anode materials for LIBs.

2 Experimental section

2.1 Synthesis of materials

SC-MWCNTs were synthesized using the floating catalyst chemical vapor deposition (CVD) method described in previous publications. [45–47] Briefly, a pyridine/ferrocene was used as the feedstock, and the CVD process was performed in a quartz tube reactor at 800 °C using N_2 as the carrier gas. Annealing of the raw, as-produced N-MWCNTs was performed in a capped graphite crucible in a helium-purged furnace. The furnace was ramped from room temperature to the target temperature (2,800 °C) at a rate of 50 °C min^{-1} under a flowing helium atmosphere kept slightly above the atmospheric pressure. Samples were held at 2,800 °C for 1 h before being cooled to room temperature at 50 °C min^{-1}. This process removes the nitrogen and the residual catalyst, anneals the graphite, [48] but does not change the apparent stacked-cup morphology of the nanotubes. We denote these nitrogen-free materials as SC-MWCNTs.

2.2 Electrochemical performance

A slurry consisting of 75 wt% SC-MWCNTs, 15 wt% sodium carboxymethyl cellulose (NaCMC) binder (Alfa Aesar), and 10 wt% conducting additive (carbon black, Super C65, Timcal) suspended in deionized water, was coated on Cu foils. After drying at 90 °C for 12 h, samples with proper size were punched from the coated foil and used as the working electrodes (WEs). The counter electrodes (CEs) were pure Li metal foils (99.9 %, Alfa Aesar), and the electrolyte was a solution of 1 M $LiPF_6$ dissolved in ethylene carbonate/dimethyl carbonate (EC/DMC, 1:1

by vol., Novolyte). The WEs and CEs were separated by polypropylene separators (Celgard 3501). CR2025 coin cells were assembled in an argon-filled glove box (MBraun) where the oxygen and moisture content were both maintained below 0.1 ppm.

Galvanostatic cycling of coin cells was conducted using a potentiostat (Bio-Logic, MPG2) with cut-off potentials of 1.5 and 0.02 V. Cycling rates were calculated based on the theoretical capacity of graphite, and 1 C corresponds to a specific current of 372 mA g^{-1} of the active materials. EIS was conducted using a potentiostat (Bio-Logic, VMP3) with the two-electrode coin cells. Before each EIS measurement, the cell was held at the designated potential until the current fell below 0.372 mA g^{-1}. The amplitude of the AC signal applied to the electrodes was 10 mV and the frequency was varied from 10^6 to 5×10^{-3} Hz.

2.3 Materials characterization

SC-MWCNTs were characterized by means of scanning electron microscopy (SEM, Hitachi S-4300), high-resolution transmission electron microscopy (HRTEM, JEOL 2010F), Raman spectroscopy (Thermo Scientific DXR Smart Raman, 532 nm laser excitation), X-ray powder diffraction analysis (XRD, Bruker D8 DISCOVER with Cu Kα radiation), and X-ray photoelectron spectroscopy (XPS, Physical Electronics PHI 5400 spectrometer with Mg X-ray source). For ex-situ Raman characterization of electrodes, WEs consisting of 85 wt% SC-MWCNT and 15 wt% NaCMC were used in the cells in order to eliminate the influence of carbon black on Raman signals. For TEM characterization, SC-MWCNT directly loaded on Cu meshes were used as the WEs. The cycled cells were disassembled in glove box and the WEs were rinsed in DMC (99 %, Alfa Aesar) before Raman and TEM tests.

3 Results and discussion

3.1 Morphology and structure

Figure 1a shows the morphology of SC-MWCNTs as obtained by HRTEM. The SC-MWCNTs produced in this work have a structure with the appearance of stacked cups and periodically bridged central cores surrounded by a thick outer wall, different from a previous reported CNT [49]. In this arrangement, the axes of graphene planes are not parallel to tube axis; thus, each graphene sheet must terminate at the surface. The average diameter and length of SC-MWCNTs are 80 nm and 17 μm, respectively, smaller than a previous reported MWCNT. [49] The incline angle between graphitic layers and the MWCNT axes are between 2° and 4°.

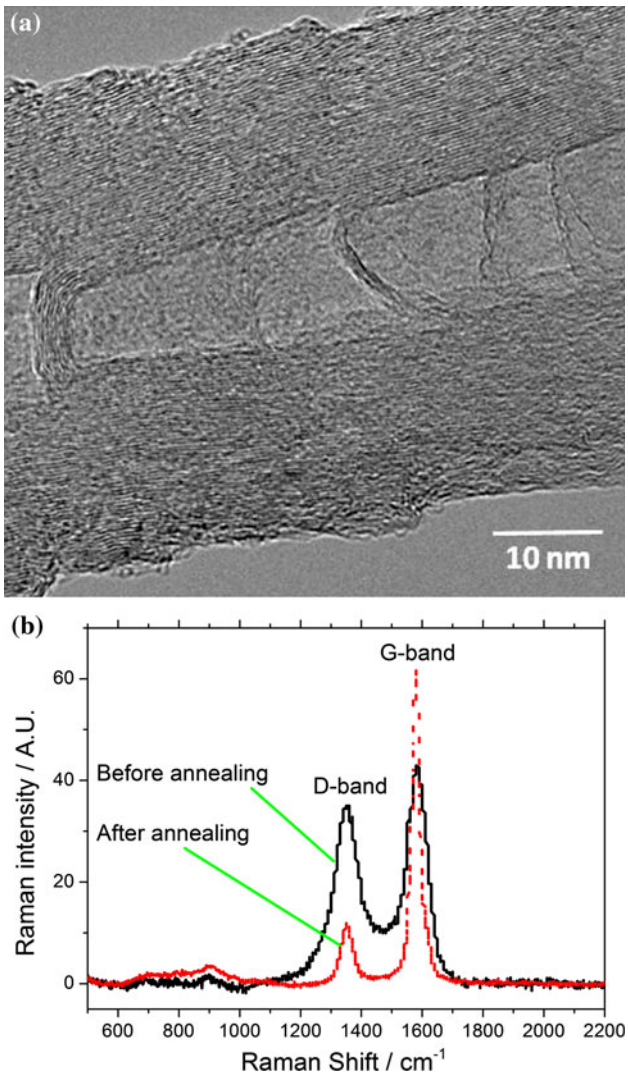

Fig. 1 **a** HRTEM image of SC-MWCNT. **b** Raman spectra of SC-MWCNTs

The degree of order of the graphitic layers within the SC-MWCNTs was examined using Raman spectroscopy, as shown in Fig. 1b. Before annealing, the CNTs mainly consist of disordered carbon and the ratio of intensities of the D-band to the G-band (I_D/I_G) is 0.82. After annealing at 2,800 °C for 1 h, the ratio of intensities decreases to 0.2, clearly indicating that high-temperature graphitization reduces the defect density, producing more perfect graphitic structure [50].

The XRD pattern of SC-MWCNTs is shown in Fig. 2a. The sharp peak at a 2θ value of 26.2° illustrates that the average interlayer spacing is 3.39 Å, in a good agreement with crystalline graphite (3.35 Å) [51]. The average grain size is calculated to be 10.7 nm according to Scherrer equation. The degree of graphitization (g value) is calculated to be 58 % based on d-spacing of (002) planes [52]. The broad asymmetric peak around 43° results from a

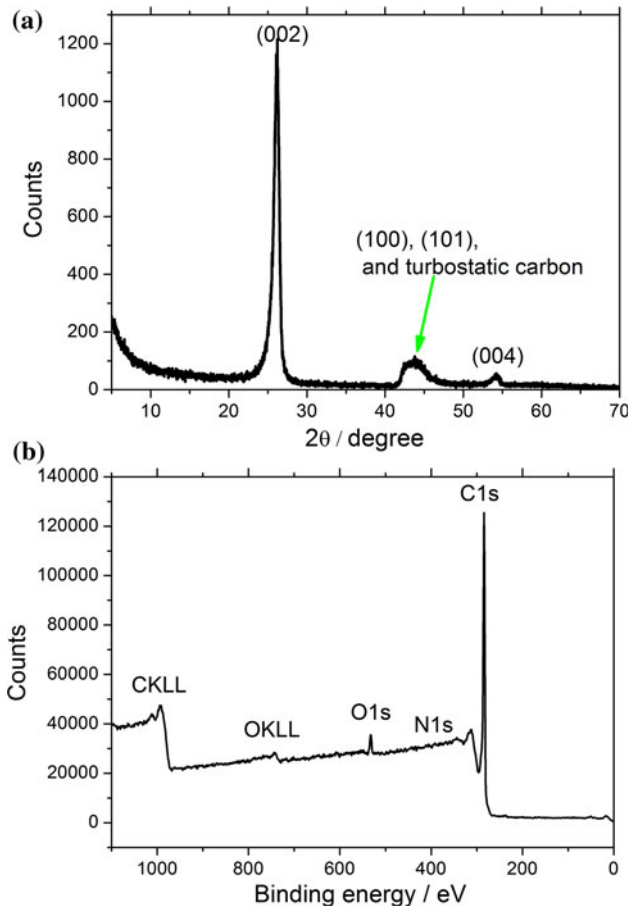

Fig. 2 **a** XRD and **b** XPS spectra of SC-MWCNTs

small amount of turbostratic structure of SC-MWCNT [53] overlapping with (100) and (101) planes of graphite. XPS spectrum (Fig. 2b) demonstrates that after annealing the material is nearly pure carbon with $\sim$3 % oxygen and virtually no nitrogen.

3.2 Lithium storage in SC-MWCNTs

The morphology of WEs consisting of SC-MWCNTs as the active materials is shown in Fig. 3. The white particles in Fig. 3 are the NaCMC binder. After coating and drying, the SC-MWCNTs form a uniform, interconnected layer with no obvious orientation preference. Figure 4a compares the galvanostatic potential-capacity profiles of lithiation and de-lithiation of SC-MWCNTs at the 1st, 2nd, and 70th cycle. The cycling rates are C/10 for 1st and 2nd cycles, and C/5 for 70th cycle. The initial reversible capacity of SC-MWCNTs under C/10 is $\sim$345 mAh g^{-1}, larger than the practical reversible capacity of graphite (310 mAh g^{-1}). The irreversible capacity at 1st cycle is 158 mAh g^{-1}, which is mainly due to the irreversible formation of a solid electrolyte interphase (SEI) layer on the electrode surface, as well as possible structural re-arrangements in the

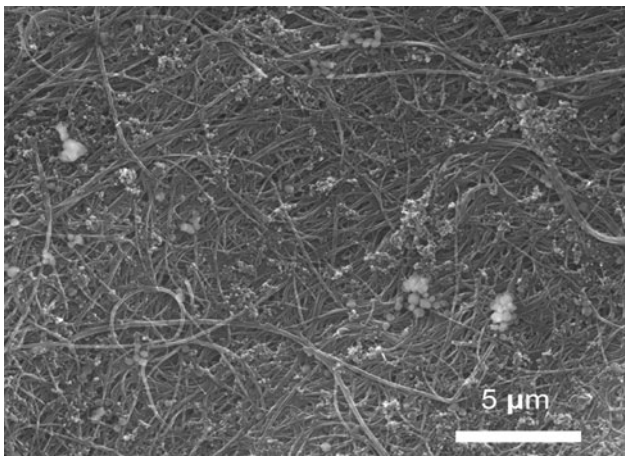

Fig. 3 SEM image of electrode after coating. The *white* particles are NaCMC binders

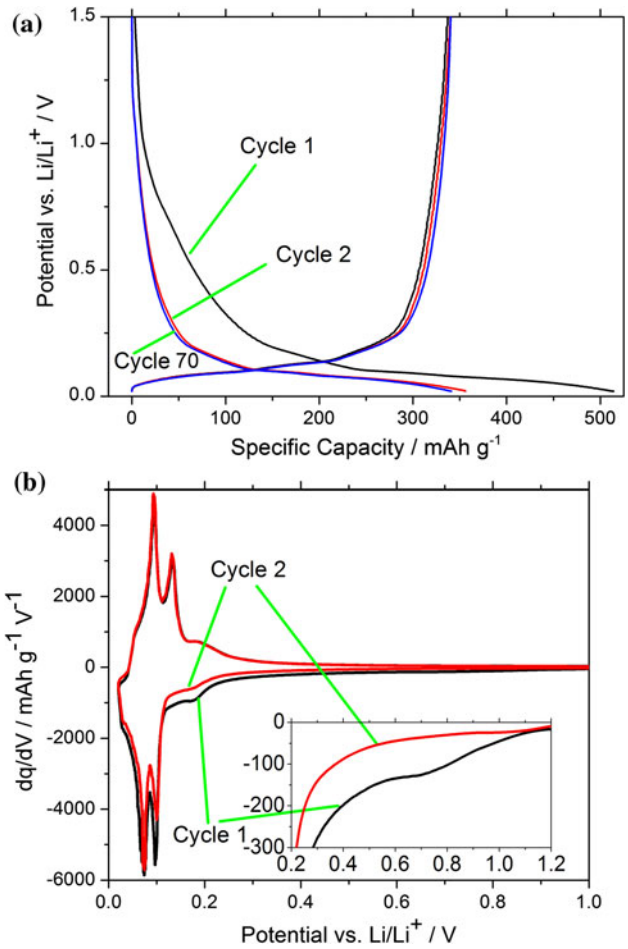

Fig. 4 **a** Constant current potential-capacity profile of Li in SC-MWCNT at selective cycles. **b** Differential potential-capacity profile of SC-MWCNT

electrode material and side reactions. The electrochemical potential range for SEI formation is clearer in differential potential-capacity profiles, as shown in Fig. 4b. Comparing

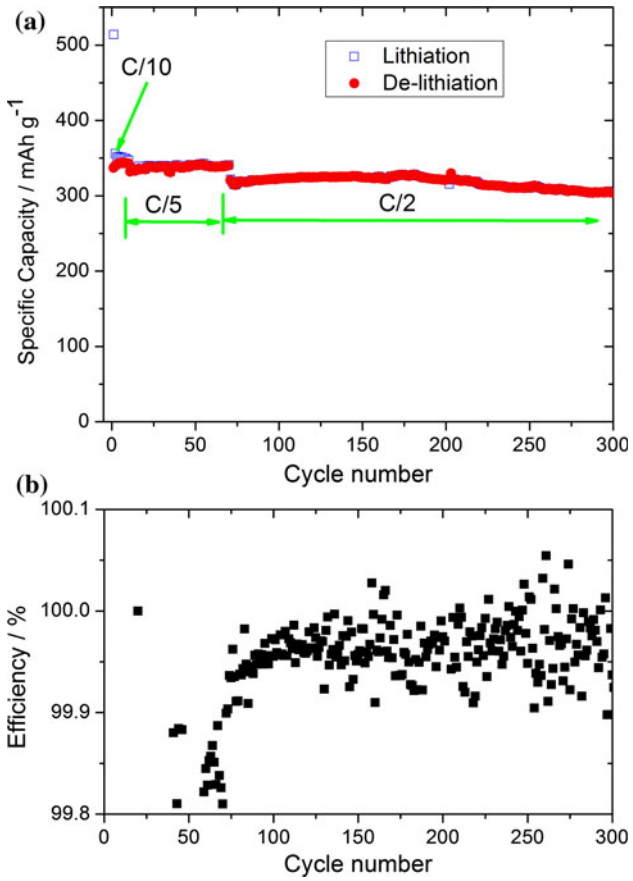

Fig. 5 Constant current cycling performance of SC-MWCNTs/Li half cells. **a** Specific discharge/charge capacities. **b** Coulombic efficiency

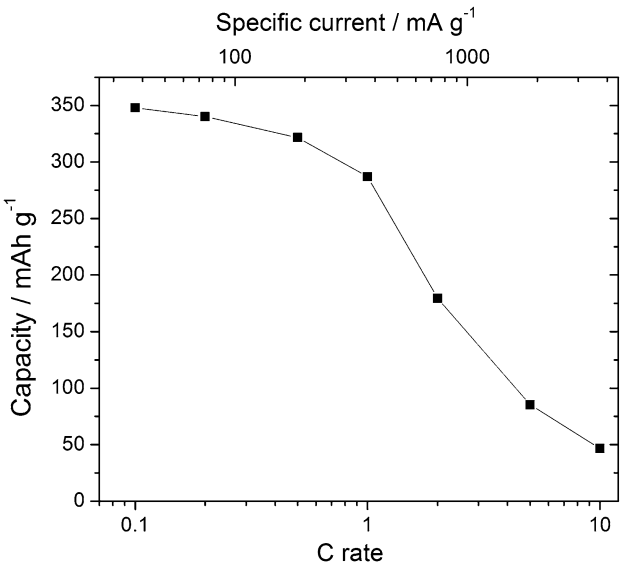

Fig. 6 Reversible capacity of SC-MWCNT at different rates. C rates are calculated based on the theoretical capacity of graphite and 1 C refers to a specific current of 372 mA g^{-1}

the discharge (lithiation) curves at the 1st and 2nd cycles, SEI formation on SC-MWCNTs occurs mainly in the range of 1.0–0.1 V versus Li/Li^+, with a peak at about 0.7 V (inset of Fig. 4b), consistent with observed potential range for SEI formation on carbonaceous materials [54, 55]. For the SC-MWCNTs produced in this work, the SEI is formed nearly completely during 1st lithiation and does not decompose readily. After the 1st lithiation, the electrochemical performance of SC-MWCNTs is so stable that the potential-capacity profiles of de-lithiation at 1st and 2nd cycles overlap with each other (Fig. 4b). Although it has been reported that iron oxide can react with Li, [56] no signal due to iron oxides is observed in Fig. 4, indicating that the electrochemical contribution from the catalyst is negligible.

The mechanism of lithiation and de-lithiation of SC-MWCNTs can be drawn from differential capacity profiles (Fig. 4b). Because SC-MWCNTs have a structure that is primarily well-stacked graphite, the three reduction peaks (0.180, 0.100, and 0.075 V) and the corresponding oxidation peaks (0.192, 0.134, and 0.097 V) occur at the similar potentials to processes in graphite electrodes, [57] which follow a reaction mechanism of

$$LiC_{72} \rightleftarrows LiC_{36} \cdots LiC_{18} \rightleftarrows LiC_{12} \rightleftarrows LiC_6 \quad (1)$$

However, compared to pure graphite, [57] the peaks in differential capacity curves are broader, which is mainly because of the small amount of disordered carbon in SC-MWCNTs, as confirmed by Raman and XRD data in Figs. 1b and 2a, respectively.

The SC-MWCNTs in this work show very stable reversible capacity upon extended cycling, as shown in Fig. 5a. The reversible capacity of the 11th cycle is 336 mAh g^{-1}, and shows essentially no decrease up to 70 cycles under a cycling rate of C/5. The capacity remains more than 300 mAh g^{-1} after 300 cycles under an accelerated cycling rate of C/2. Note the Columbic efficiency upon extended cycling is greater than 99.9 % (Fig. 5b), which is considered excellent in early stage of materials R&D. High coulombic efficiency is needed by advanced LIBs for EVs, whose cycle life is required to be as long as 5,000 cycles. Thus, SC-MWCNTs fabricated herein are candidate materials for LIB anodes.

The constant current cycling performance of SC-MWCNTs under different rates is summarized in Fig. 6. The reversible capacity of SC-MWCNTs is 348, 340, 322, and 287 mAh g^{-1} for cycling rate of C/10, C/5, C/2, and 1C, respectively. However, when the cycling rate goes up to 2 C, the capacity is only 180 mAh g^{-1}, and drops to less than 100 mAh g^{-1} at rates faster than 5 C. This indicates that the performance of SC-MWCNTs at high rates is not ideal. However, these materials can be used at rates of up to

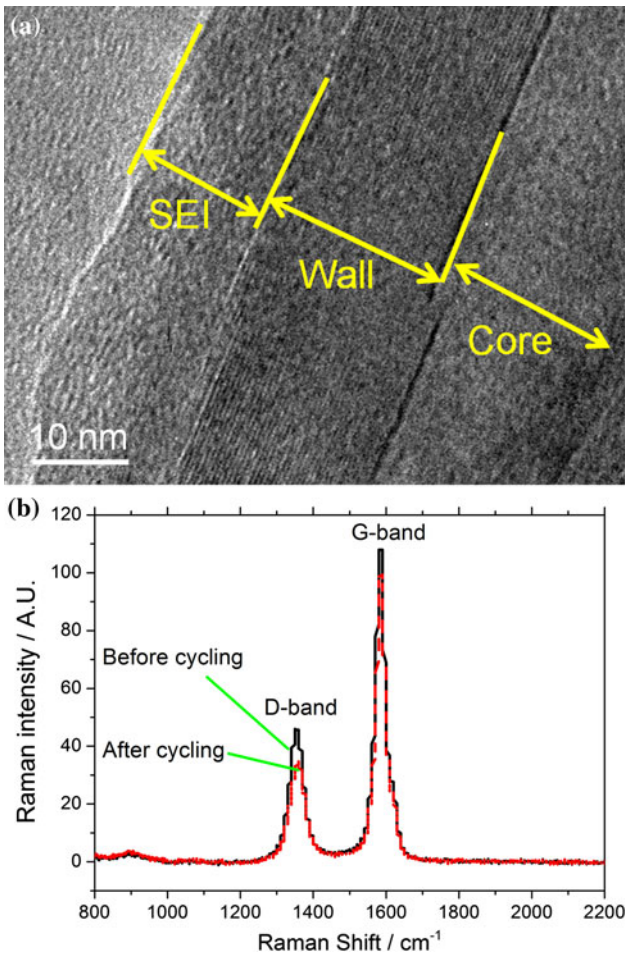

Fig. 7 **a** Ex-situ TEM image of SC-MWCNT after 80 cycles. **b** Ex-situ Raman spectra of SC-MWCNT before cycling and after 50 cycles

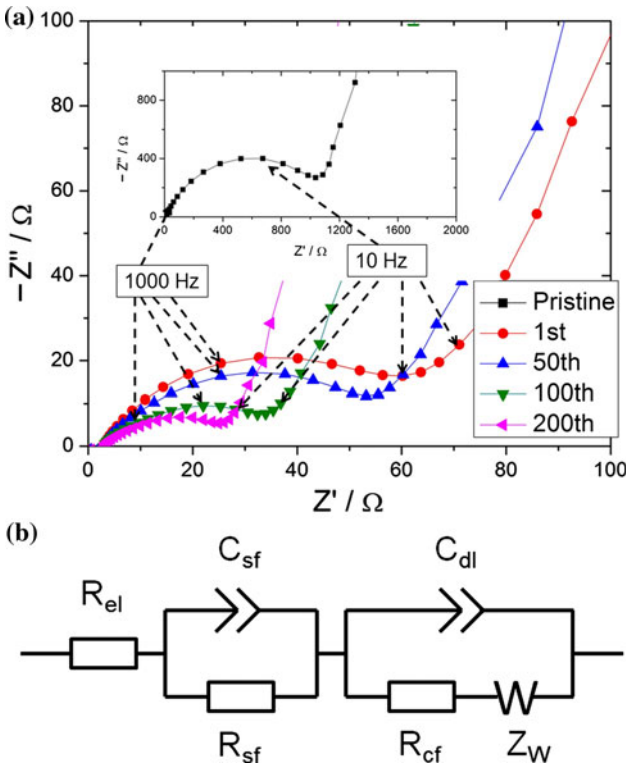

Fig. 8 **a** Nyquist plots of EIS spectra of SC-MWCNTs at different cycle numbers. **b** The equivalent circuit used to simulate the EIS spectra

1 C, which are practical for low power applications. Reducing the average length of SC-MWCNTs, and thus the mean diffusion distance for lithium could possibly enhance the performance of the anodes at a higher rate.

3.3 Structure of SC-MWCNT after cycling

In order to examine the materials stability after electrochemical tests, ex-situ TEM, and Raman spectroscopy were conducted on dissected coin cell electrodes. A TEM image of SC-MWCNT after 80 cycles is shown in Fig. 7a. After cycling, the SC-MWCNTs retain their original layered-graphitic structure and there is no evidence of mechanical degradation or surface damage. A uniform layer of SEI formed on the surface of MWCNTs, which has a thickness of about 15 nm.

Ex-situ Raman spectra of SC-MWCNTs before and after 50 cycles are shown in Fig. 7b. The average I_D/I_G ratio is 0.34 after 50 cycles, which was 0.37 before cycling. Raman spectroscopy results indicate that the structure of SC-MWCNTs is stable and does not change significantly during extended electrochemical cycling.

3.4 EIS measurement

To further explore the reason for the observed stable cycling performance of SC-MWCNTs, EIS was carried out at different cycle numbers in the charged state (1.5 V vs. Li/Li^+). Nyquist plots derived from the analyses are shown in Fig. 8a. The inset in Fig. 8a shows the impedance of SC-MWCNTs anode before cycling. As seen from the figure, the ac impedance spectra mainly consist of a depressed semicircle at high and medium frequency regions, and an arc at low frequency region. The convoluted semicircle represents the combination of impedance due to surface SEI film and charge transfer through the electrode/electrolyte interface [58]. The arc represents solid-state diffusion behavior.

To quantify the EIS spectra, we use an equivalent circuit to fit the EIS response, as shown in Fig. 8b. In this equivalent circuit, R_{el} is resistance due to the electrolyte, R_{sf} is surface film (SEI) resistance, R_{cf} is the resistance due to the charge-transfer process, C_{sf} is a constant phase element (CPE) due to a surface film or SEI layer, C_{dl} is the double layer capacitance, and Z_W represents the Warburg diffusion behavior.

Table 1 Parameters obtained from fitting EIS data for SC-MWCNT at different cycle numbers

Cycle number	R_{el} (Ω)	R_{sf} (Ω)	C_{sf} (μF)	R_{cf} (Ω)	C_{dl} (μF)
1	2.73	54.8	49.3	8.51	2.35
50	0.87	48.9	63.6	1.70	0.85
100	1.36	31.3	66.5	1.44	4.99
200	1.76	23.0	98.4	0.99	5.14

Values of resistance and capacitance based on fitting EIS data using the equivalent circuit are shown in Table 1. As seen here, resistance and capacitance corresponding to surface film and charge transfer are relatively stable up to 200 cycles. Trends of slight decrease in R_{sf} and R_{cf} and slight increase in C_{sf} and C_{dl} can be seen with cycling. A possible reason is given here: because of the structural stability of SC-MWCNT, the SEI film that is mainly composed of two layers, a dense inorganic layer next to the electrode materials and a porous organic layer next to the electrolyte [59–62], does not crack during cycling. With further cycling, the porosity in the organic top layer tends to increase, [54, 60, 63] leading to larger surface area of SEI; thus, the overall resistance decreases and capacitance increases.

4 Conclusions

Here we synthesized stacked-cup-type MWCNTs using a floating catalyst CVD method. Electrochemical measurements show that SC-MWCNTs deliver a stable capacity of $\sim$310 mAh g^{-1} at a rate of C/2 to 300 cycles and superb columbic efficiency that is greater than 99.9 %. The SC-MWCNTs consist of a layered graphitic structure with a small amount of turbostratic carbon, which remain unchanged upon extended electrochemical cycles of lithiation and de-lithiation. Good structural stability and a stable SEI layer, as confirmed by ex-situ TEM and Raman spectroscopy, are the main reasons for the stable cycling behavior, as well as for the characteristics of the EIS measurements. A possible mechanism was proposed for the slight decrease in surface film resistance observed in the EIS. The results suggest that the SC-MWCNTs produced in this work are candidate materials for LIB anodes. They may also be used as conducting additives and for composite electrodes.

Acknowledgments J.C.L. and Y.T.C. are grateful to financial support from NSF (CMMI #1000726) and General Motors. M.S.M. and A.P.K. wish to thank Dali Qian and Center for Applied Energy Research, University of Kentucky for producing starting CNTs and to thank Dr. Per Askeland and Dr. Doo Young Kim for XPS analysis.

References

1. Armand M, Tarascon JM (2008) Building better batteries. Nature 451(7179):652–657
2. Zhu Y, Li Y, Bettge M, Abraham DP (2012) Positive electrode passivation by LiDFOB electrolyte additive in high-capacity lithium-ion cells. J Electroceram Soc 159(12):A2109–A2117
3. Zhu Y, Matthew Casselman D, Li Y, Wei A, Daniel Abraham P (2013) Perfluoroalkyl-substituted ethylene carbonates: novel electrolyte additives for high-voltage lithium-ion batteries. J Power Sour 232:23–28
4. van Schalkwijk WA, Scrosati B (2002) Advances in lithium-ion batteries, vol x. Kluwer Academic/Plenum, New York, p 513
5. Nazri G, Pistoia G (2004) Lithium batteries : science and technology, vol xix. Kluwer Academic, Boston, p 708
6. Zhu Y, Li Y, Bettge M, Daniel Abraham P (2013) Electrolyte additive combinations that enhance performance of high-capacity Li1.2Ni0.15Mn0.55Co0.1O2–graphite cells. Electrochimica Acta 233:346e357
7. Cheng YT, Verbrugge MW (2010) Diffusion-induced stress, interfacial charge transfer, and criteria for avoiding crack initiation of electrode particles. J Electrochem Soc 157(4):A508–A516
8. Cheng YT, Verbrugge MW (2009) Evolution of stress within a spherical insertion electrode particle under potentiostatic and galvanostatic operation. J Power Sour 190(2):453–460
9. Li JC, Dozier AK, Li YC, Yang FQ, Cheng YT (2011) Crack pattern formation in thin film lithium-ion battery electrodes. J Electrochem Soc 158(6):A689–A694
10. Harris PJF (2009) Carbon nanotube science : synthesis, properties and applications. Rev. and updated, vol x. Cambridge University Press, Cambridge, New York, p 301
11. Gong QJ, Li HJ, Wang X, Fu QG, Wang ZW, Li KZ (2007) In situ catalytic growth of carbon nanotubes on the surface of carbon cloth. Compos Sci Technol 67(14):2986–2989
12. Centi G, Perathoner S (2011) Carbon nanotubes for sustainable energy applications. ChemSusChem 4(7):913–925
13. Che G, Lakshmi BB, Fisher ER, Martin CR (1998) Carbon nanotubule membranes for electrochemical energy storage and production. Nature 393(6683):346
14. Frackowiak E, Béguin F (2002) Electrochemical storage of energy in carbon nanotubes and nanostructured carbons. Carbon 40(10):1775–1787
15. Shin H-C, Liu M, Sadanadan B, Rao AM (2002) Electrochemical insertion of lithium into multi-walled carbon nanotubes prepared by catalytic decomposition. J Power Sour 112(1):216–221
16. Wang GX, Ahn J-H, Yao J, Lindsay M, Liu HK, Dou SX (2003) Preparation and characterization of carbon nanotubes for energy storage. J Power Sour 119–121:16–23
17. Lv R, Zou L, Gui X, Kang F, Zhu Y, Zhu H, Wei J, Gu J, Wang K, Wu D (2008) High-yield bamboo-shaped carbon nanotubes from cresol for electrochemical application. Chem Commun 17:2046–2048
18. Nishidate K, Hasegawa M (2005) Energetics of lithium ion adsorption on defective carbon nanotubes. Phys Rev B 71(24): 245418
19. Song B, Yang J, Zhao J, Fang H (2011) Intercalation and diffusion of lithium ions in a carbon nanotube bundle by ab initio molecular dynamics simulations. Energy Environ Sci 4(4):1379–1384
20. Eom JY, Kwon HS, Liu J, Zhou O (2004) Lithium insertion into purified and etched multi-walled carbon nanotubes synthesized on supported catalysts by thermal CVD. Carbon 42(12–13):2589–2596
21. Wang XX, Wang JN, Chang H, Zhang YF (2007) Preparation of short carbon nanotubes and application as an electrode material in Li-ion batteries. Adv Funct Mater 17(17):3613–3618

22. Wang XX, Wang JN, Su LF (2009) Preparation and electrochemical performance of ultra-short carbon nanotubes. J Power Sour 186(1):194–200
23. Welna DT, Liangti Qu, Taylor BE, Dai L, Durstock MF (2011) Vertically aligned carbon nanotube electrodes for lithium-ion batteries. J Power Sour 196(3):1455–1460
24. Lin K, Yanhui Xu, He G, Wang X (2006) The kinetic and thermodynamic analysis of Li ion in multi-walled carbon nanotubes. Mater Chem Phys 99(2–3):190–196
25. Zhao M, Xia Y, Mei L (2005) Diffusion and condensation of lithium atoms in single-walled carbon nanotubes. Phys Rev B 71(16):165413
26. Liu Y, Zheng He, Hua Liu X, Huang S, Zhu T, Wang J, Kushima A, Hudak NS, Huang X, Zhang S, Mao SX, Qian X, Li J, Yu Huang J (2011) Lithiation-induced embrittlement of multiwalled carbon nanotubes. ACS Nano 5(9):7245–7253
27. Zhong DY, Zhang GY, Liu S, Wang EG, Wang Q, Li H, Huang XJ (2001) Lithium storage in polymerized carbon nitride nanobells. Appl Phys Lett 79(21):3500–3502
28. Wang Q, Li H, Chen L, Huang X, Zhong D, Wang E (2003) Investigation of lithium storage in bamboo-like CNTs by HRTEM. J Electrochem Soc 150(9):A1281–A1286
29. Zou L, Lv R, Kang F, Gan L, Shen W (2008) Preparation and application of bamboo-like carbon nanotubes in lithium ion batteries. J Power Sour 184(2):566–569
30. Landi BJ, Dileo RA, Schauerman CM, Cress CD, Ganter MJ, Raffaelle RP (2009) Multi-walled carbon nanotube paper anodes for lithium ion batteries. J Nanosci Nanotechnol 9(6):3406–3410
31. Bulusheva LG, Okotrub AV, Kurenya AG, Zhang H, Zhang H, Chen X, Song H (2011) Electrochemical properties of nitrogen-doped carbon nanotube anode in Li-ion batteries. Carbon 49(12):4013–4023
32. Li X, Liu J, Zhang Y, Li Y, Liu H, Meng X, Yang J, Geng D, Wang D, Li R, Sun X (2012) High concentration nitrogen doped carbon nanotube anodes with superior Li+ storage performance for lithium rechargeable battery application. J Power Sour 197: 238–245
33. Guo BK, Wang XQ, Fulvio PF, Chi MF, Mahurin SM, Sun XG, Dai S (2011) Soft-templated mesoporous carbon–carbon nanotube composites for high performance lithium-ion batteries. Adv Mater 23(40):4661–4666
34. Martha SK, Nanda J, Veith GM, Dudney NJ (2012) Electrochemical and rate performance study of high-voltage lithium-rich composition: $Li_{1.2}Mn_{0.525}Ni_{0.175}Co_{0.1}O_2$. J Power Sour 199: 220–226
35. Ahn D, Xiao X, Li Y, Sachdev AK, Park HW, Yu A, Chen Z (2012) Applying functionalized carbon nanotubes to enhance electrochemical performance of tin oxide composite electrodes for Li-ion battery. J Power Sour 212:66–72
36. Yang JL, Wang JJ, Li XF, Wang DN, Liu J, Liang GX, Gauthier M, Li YL, Geng DS, Li RY, Sun XL (2012) Hierarchically porous LiFePO4/nitrogen-doped carbon nanotubes composite as a cathode for lithium ion batteries. J Mater Chem 22(15):7537–7543
37. Guo JC, Xu YH, Wang CS (2011) Sulfur-impregnated disordered carbon nanotubes cathode for lithium–sulfur batteries. Nano Lett 11(10):4288–4294
38. Marschilok A, Lee C-Y, Subramanian A, Takeuchi KJ, Takeuchi ES (2011) Carbon nanotube substrate electrodes for lightweight, long-life rechargeable batteries. Energy Environ Sci 4(8):2826–2830
39. Li X, Kang F, Bai X, Shen W (2007) A novel network composite cathode of LiFePO4/multiwalled carbon nanotubes with high rate capability for lithium ion batteries. Electrochem Commun 9(4):663–666
40. Li X, Kang F, Shen W (2006) A comparative investigation on multiwalled carbon nanotubes and carbon black as conducting additive in LiNi[sub 0.7]Co[sub 0.3]O[sub 2]. Electrochem Solid-State Lett 9(3):A126–A129
41. Li X, Kang F, Shen W (2006) Multiwalled carbon nanotubes as a conducting additive in a LiNi0.7Co0.3O2 cathode for rechargeable lithium batteries. Carbon 44(7):1334–1336
42. Sheem K, Lee YH, Lim HS (2006) High-density positive electrodes containing carbon nanotubes for use in Li-ion cells. J Power Sour 158(2):1425–1430
43. Wang G, Li H, Zhang Q, Zuolong Y, Meizheng Q (2011) The study of carbon nanotubes as conductive additives of cathode in lithium ion batteries. J Solid State Electrochem 15(4):759–764
44. Katar SL, Hernandez D, Labiosa AB, Mosquera-Vargas Ed, Fonseca L, Weiner B, Morell G (2010) SiN/bamboo like carbon nanotube composite electrodes for lithium ion rechargeable batteries. Electrochim Acta 55(7):2269–2274
45. Qian D, Andrews R, Jacques D, Kichambare P, Lian G, Dickey EC (2003) Low-temperature synthesis of large-area CN*x* nanotube arrays. J Nanosci Nanotech 3:93–97
46. Meier MS, Selegue JP, Cassity KB, Kaur AP, Qian DL (2010) Linear and spiral forms of longitudinal cuts in graphitized N-doped multiwalled carbon nanotubes (g-N-MWCNTs). J Phys-Condensed Matter 22(33):334219
47. Meier MS, Andrews R, Jacques D, Cassity KB, Qian D (2008) Tearing open nitrogen-doped multiwalled carbon nanotubes. J Mater Chem 18(35):4143–4145
48. Andrews R, Jacques D, Qian D, Dickey EC (2001) Purification and structural annealing of multiwalled carbon nanotubes at graphitization temperatures. Carbon 39:1681–1687
49. Alcántara R, Lavela P, Ortiz GF, Tirado JL, Zhecheva E, Stoyanova R (2007) Lithium insertion into modified conducting domains of graphitized carbon nanotubes. J Electrochem Soc 154(10):A964–A970
50. Bom D, Andrews R, Jacques D, Anthony J, Chen B, Meier MS, Selegue JP (2002) Thermogravimetric analysis of the oxidation of multiwalled carbon nanotubes: evidence for the role of defect sites in carbon nanotube chemistry. Nano Lett 2:615–619
51. Shioyama H (2000) The interactions of two chemical species in the interlayer spacing of graphite. Synth Met 114(1):1–15
52. Zou L\, Huang B\, Huang Y, Huang Q, Wang C (2003) An investigation of heterogeneity of the degree of graphitization in carbon–carbon composites. Mater Chem Phys 82(3):654–662
53. Nalimova VA, Sklovsky DE, Bondarenko GN, AlvergnatGaucher H, Bonnamy S, Beguin F (1997) Lithium interaction with carbon nanotubes. Synth Met 88(2):89–93
54. Verma P, Maire P, Novak P (2010) A review of the features and analyses of the solid electrolyte interphase in Li-ion batteries. Electrochim Acta 55(22):6332–6341
55. Winter M, Besenhard JO, Spahr ME, Novak P (1998) Insertion electrode materials for rechargeable lithium batteries. Adv Mater 10(10):725–763
56. Alcántara R, Lavela P, Ortiz GF, Tirado JL, Stoyanova R, Zhecheva E, Merino C (2004) Nanodispersed iron, tin and antimony in vapour grown carbon fibres for lithium batteries: an EPR and electrochemical study. Carbon 42(11):2153–2161
57. Ohzuku T, Iwakoshi Y, Sawai K (1993) Formation if lithium–graphite intercalation compounds in nonaqueous electrolytes and their application as a negative electrode for a lithium ion (Shuttlecock) cell. J Electrochem Soc 140(9):2490–2498
58. Gregorio F, Ortiz RA, Lavela P, Tirado JL (2005) Optimization of the electrochemical behavior of vapor grown carbon nanofibers for lithium-ion batteries by impregnation, and thermal and hydrothermal treatments. J Electrochem Soc 152(9):A1797–A1803
59. Xiao XC, Lu P, Ahn D (2011) Ultrathin multifunctional oxide coatings for lithium ion batteries. Adv Mater 23(34):3911

60. Winter M (2009) The solid electrolyte interphase: the most important and the least understood solid electrolyte in rechargeable Li batteries. Zeitschrift Fur Physikalische Chemie 223(10–11):1395–1406
61. Shkrob IA, Zhu Y, Marin TW, Abraham D (2013) Reduction of carbonate electrolytes and the formation of solid-electrolyte interface (SEI) in lithium ion batteries. 1. Spectroscopic observations of radical intermediates generated in one-electron reduction of carbonates. J Phys Chem C
62. Shkrob IA, Zhu Y, Marin TW, Abraham D (2013) Reduction of carbonate electrolytes and the formation of solid-electrolyte interface (SEI) in lithium batteries. 2. Radiolytically induced polymerization of ethylene carbonate. J Phys Chem C
63. Aurbach D (2000) Review of selected electrode-solution interactions which determine the performance of Li and Li ion batteries. J Power Sour 89(2):206–218